Spanwise Variation of Laminar Separation Bubbles on Wings at Low Reynolds Numbers

William G. Bastedo Jr.* and Thomas J. Mueller†
University of Notre Dame, Notre Dame, Indiana

The Wortmann FX63-137 airfoil section and three rectangular wings that used this section were studied at chord Reynolds numbers ranging from 80,000 to 200,000 to determine the effect of the laminar separation bubbles on performance and the spanwise variation in the bubbles due to the influence of the tip vortex. It was found that increasing the chord Reynolds number increased the performance of both the airfoil and the wings while decreasing the aspect ratio decreased wing performance. Determination of the interaction of the tip vortex with the separation bubble was attempted. Flow visualization data were compared to chordwise static pressure distributions obtained at seven stations along the span for the $\mathcal{R}=2.0$ case. Both sets of data showed that the tip vortex reduced the local angle of attack along the span. Comparison of pressure distributions showed that the flowfield at spanwise stations on the wings were identical to two-dimensional distributions at the equivalent effective angle of attack.

Nomenclature

$\mathcal{R}$ = semispan aspect ratio, based on the distance from model root to tip b, $=b^2/S$
b = semispan length, distance from model root to tip, cm
c = chord length of wing or airfoil model, cm
C_d = airfoil section profile drag coefficient
C_D = wing drag coefficient
C_l = airfoil section lift coefficient
C_L = wing lift coefficient
C_p = pressure coefficient, $=(P_i-P_\infty)/Q$
P = static pressure, mm H_2O
Q = dynamic pressure, $\frac{1}{2}\rho U_\infty^2$
R_c = Reynolds number based on airfoil or wing chord length
S = airfoil or wing planform area, $=b\cdot c$ for all cases
U = velocity in the streamwise direction
α = angle of attack, deg
μ = absolute viscosity, kg/m·s
ρ = density of air, kg/m^3

Subscripts

i = pressure-tap location i, also used to denote induced (by tip vortex) effect
∞ = wind tunnel freestream condition

Introduction

RECENTLY, a large number of flight vehicles have been developed that operate at chord Reynolds numbers less than 500,000. Examples of such aircraft are high-altitude, remotely piloted vehicles; low-altitude, low-velocity mini-RPV's; man-powered flight systems; and ultralight recreational aircraft. Previous studies have concentrated on determining two-dimensional airfoil performance at chord Reynolds numbers less than 500,000 and have shown that the formation of laminar separation bubbles usually had major impact on aerodynamic performance.[1-4] It must then be suspected that separation bubbles have a significant influence on wing performance in the low Reynolds number regime.

The laminar separation bubble has been studied on two-dimensional geometries for many years, but it is still not completely understood. Because of the sensitivity of the boundary layer at low Reynolds numbers, accurate experimental data are difficult to obtain. Intrusive measurement techniques (i.e., hot-wire anemometry, static-pressure measurements, and surface visualization techniques) have been observed to modify the flowfield, and the resulting data are often confusing and must be interpreted with great care.[5,6] Because of certain limitations inherent to the problem, it was necessary to use intrusive testing techniques in this study. The effects of these problems will be discussed later in the paper. As a result of many previous studies, the important physical parameters that affect formation of laminar separation bubbles have been determined to be the airfoil geometry, angle of attack, chord Reynolds number, and freestream disturbance environment.

Historically, laminar separation bubbles have been classified as either "long" or "short." Long bubbles may be as much as 20–30% of the chord in length and adversely affect airfoil performance.[7] On the other hand, short bubbles are usually only a few percent of the chord in length, causing very little modification of the pressure distribution. These bubbles serve primarily as a tripping mechanism to allow reattachment of an otherwise separated shear layer and increase performance. Associated with this, a long bubble tends to increase in length as incidence is increased, decreasing the slope of the lift curve. A short bubble, on the other hand, decreases in length with increasing angle of attack, yielding improved airfoil performance.

Wing aerodynamics have been studied for quite some time, and high Reynolds number cases have been modeled quite successfully. The higher-pressure air of the lower surface leaks around the tip, forming the tip vortex on lifting wings. This vortex induces a velocity field that effectively reduces the local angle of attack along the span. Analytic techniques based on potential flow models (e.g., lifting line) have been developed and used as tools in wing design. These methods, because they are based on inviscid flow theory, do not account for the separated flow phenomena so frequently found on low

Received May 15, 1985; presented as Paper 85-1590 at the AIAA 18th Fluid Dynamics and Plasmadynamics and Lasers Conference, Cincinnati, OH, July 16-18, 1985; revision received June 27, 1986.

*Research Assistant, Department of Aerospace and Mechanical Engineering; currently Technical Staff Member, Space Station Div., Rockwell International, Downing, CA. Member AIAA.

†Professor, Department of Aerospace and Mechanical Engineering. Associate Fellow AIAA.

Reynolds number airfoils and wings. Comparison of predictive techniques and experimental data is needed to ascertain the applicability of these tools to low Reynolds number flight regime design problems.

In order to study this problem, the performance of the Wortmann FX63-137 airfoil section and a rectangular wing ($\mathcal{R}=2.0$) using that profile were studied at chord Reynolds numbers of 80,000 and 200,000. Semispan test models were mounted on a reflection plate. The airfoil coordinates are presented in Table 1. The boundary-layer characteristics of the airfoil were studied to develop an understanding of the separation bubble for the two-dimensional airfoil as a function of angle of attack. These data were then used as a reference when the data obtained at various stations along the span of the finite wing were interpreted.

Experimental Techniques

Each experiment was performed in one of the two "identical" low-speed wind tunnels located in the Notre Dame Aerospace Laboratory. These facilities were ideal for the experiments since they produced low turbulence intensities (less than 0.1%) over the entire operating range. A more complete description of the wind tunnel facilities is available in Ref. 6. The tunnel test section was 24 in. square in cross section, and all test models had 6-in. chords. The wing models were cantilevered from a reflection plate 3 in. from one test wall. This gave the $\mathcal{R}=2.0$ model a clearance of $3c/2$ from the wall. A pair of endplates were symmetrically mounted to test the airfoil model, which was the same model as the $\mathcal{R}=2.7$ case.

Aerodynamic force measurements were obtained using an externally mounted, two-component force balance, its associated electronic amplifiers, and an Apple IIe microcomputer data acquisition system. This system is shown in Fig. 1.

Static-pressure distributions were obtained using a specially constructed semispan model whose static-pressure taps were connected to a Scanivalve electronic switching box, electronic manometers, and a PDP 11/23 minicomputer, as shown in Fig. 2. This model allowed the measurement of chordwise static-pressure distributions (in-line pressure taps) at seven stations along the span of the model, as well as for the two-dimensional case, by affixing a second endplate and measuring the pressure distribution at the $y/b=54\%$ station.

Since the character, location, and length of laminar separation bubbles were of interest in this study, the chordwise positions of separation of the laminar boundary layer from the surface, transition of the free shear layer, and turbulent reattachment to the surface had to be determined. Because it was necessary to determine the character of the flowfield at various spanwise stations, it was necessary to use in-line pressure taps rather than a staggered configuration, which minimizes the effect of the upstream taps on the downstream taps.

Different forms of flow visualization were used to identify separation bubble locations. Kerosene smoke injected upstream of the contraction was illuminated by a "sheet" of laser light. This technique helped to identify the position of the separation bubble on the airfoil. A form of surface oil visualization (a propylene glycol/water mixture as the carrier and a fluorescent dye as the marker) was employed to determine spanwise variations in the separation bubble on the wing. These techniques are documented in greater detail in Ref. 6.

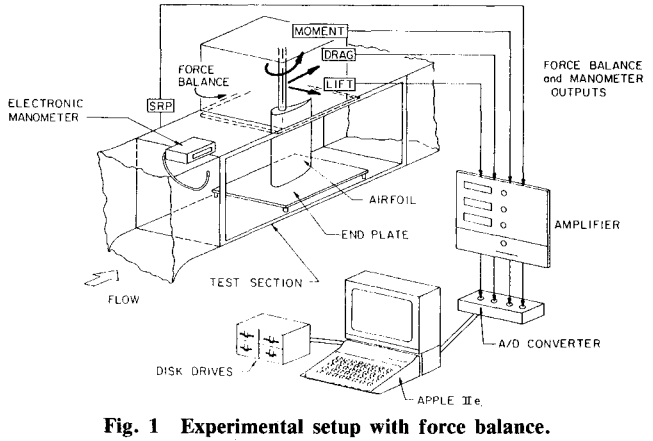

Fig. 1 Experimental setup with force balance.

Results

A large amount of data, both quantitative and qualitative, was obtained for the Wortmann FX63-137 airfoil section and three rectangular planform semispan wings ($\mathcal{R}=2.7$, 2.0, and 1.5) at chord Reynolds numbers of 80,000 and 200,000. The two-dimensional lift and drag curves are shown in Figs. 3 and 4 and are compared to the finite wing data in Figs. 5 and 6. As expected, the slopes of the lift curve decreased as aspect ratio decreased, and performance improved as Reynolds number was increased. Because of its highly nonlinear shape and the large regions of separated flow, the $R_c=80{,}000$, $\mathcal{R}=2.0$ model lift slope was not accurately predicted by the lifting-line theory. The slope of the lift curve for the $R_c=200{,}000$, $\mathcal{R}=2.0$ case was predicted fairly well.

Table 1 Wortmann FX 63-137 airfoil coordinates

X/C	Y_{upper}/C	Y_{lower}/C
0.00000	0.00000	0.00000
0.00107	0.00900	−0.00232
0.00428	0.01750	−0.00566
0.00961	0.02740	−0.00995
0.01704	0.03625	−0.01254
0.02653	0.04480	−0.01537
0.03806	0.05248	−0.01698
0.05156	0.06005	−0.01887
0.06699	0.06836	−0.01992
0.08427	0.07555	−0.02122
0.10332	0.08313	−0.02180
0.12408	0.08961	−0.02256
0.14645	0.09622	−0.02263
0.17033	0.10165	−0.02277
0.19562	0.10704	−0.02220
0.22221	0.11122	−0.02161
0.25000	0.11522	−0.02034
0.27886	0.11792	−0.01895
0.30866	0.12024	−0.01688
0.33928	0.12128	−0.01460
0.37059	0.12191	−0.01167
0.40245	0.12137	−0.00848
0.43474	0.12042	−0.00486
0.46730	0.11833	−0.00103
0.50000	0.11578	0.00307
0.53270	0.11221	0.00716
0.56526	0.10823	0.01112
0.59755	0.10331	0.01475
0.62941	0.09804	0.01813
0.66072	0.09204	0.02098
0.69134	0.08590	0.02345
0.72114	0.07927	0.02530
0.75000	0.07273	0.02668
0.77779	0.06605	0.02745
0.80438	0.05962	0.02768
0.82967	0.05323	0.02729
0.85355	0.04711	0.02631
0.87592	0.04114	0.02479
0.89668	0.03553	0.02284
0.91573	0.03018	0.02052
0.93301	0.02516	0.01794
0.94844	0.02043	0.01514
0.96194	0.01601	0.01219
0.97347	0.01189	0.00921
0.98296	0.00818	0.00630
0.99039	0.00501	0.00373
0.99572	0.00249	0.00169
0.99893	0.00082	0.00040
1.00000	0.00000	0.00000

The force data delineated airfoil and wing performance as functions of angle of attack, but very little could be inferred from this concerning boundary-layer behavior. Indications of boundary-layer separation, transition, and reattachment positions were determined by examining static-pressure distributions and flow visualization data. By comparing all the data, it was possible to infer some of the effects of the tip vortex on the separation bubbles and, subsequently, on wing performance.

Two-Dimensional Boundary-Layer Characteristics of the Wortmann FX63-137 Airfoil Section

The two-dimensional boundary-layer characteristics $R_c = 80{,}000$ proved interesting. At angles of attack less than 6-deg, laminar separation without turbulent reattachment occurred on the upper surface. As incidence was increased in this region, the separation point moved upstream and the rate of lift production decreased, much as with the performance of a flat plate that has developed a long separation bubble on the upper surface. At 6-deg angle of attack, the long bubble was abruptly transformed into a short bubble, greatly increasing lift and slightly decreasing drag (Fig. 3).

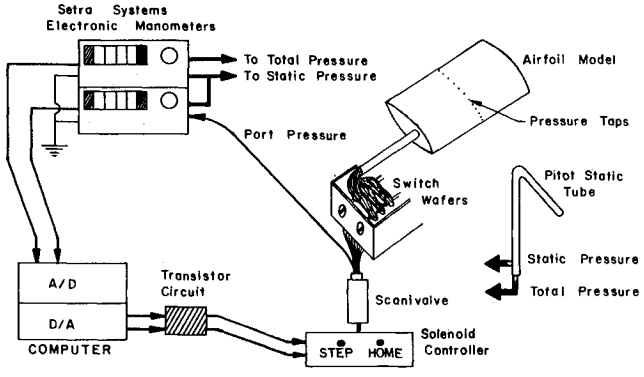

Fig. 2 System for measuring static-pressure distributions.

At angles of attack greater than 6 deg, the separation bubble moved upstream on the airfoil and decreased in length as incidence was increased. A summary of the positions of laminar separation, transition, and turbulent reattachment at $R_c = 80{,}000$ is presented in Fig. 7. As shown, the bubble decreased in length until it burst at the leading edge, causing a dramatic decrease in lift, an increase in drag, and a conventional clockwise hysteresis loop.[8]

Boundary-layer behavior for the two-dimensional case at $R_c = 200{,}000$ was much more predictable. The short bubble that formed at about 6-deg angle of attack at the lower Reynolds number formed much earlier at $R_c = 200{,}000$, eliminating the discontinuities in the force curves at $R_c = 80{,}000$. A laminar separation bubble existed on the upper surface from zero lift (-7 deg) to leading-edge separation (21 deg). The separation bubbles observed in these experiments should still be classified as short bubbles, although some were as long as 30% of the chord. As was the case at the lower Reynolds number, the bubble on the surface moved upstream toward the leading edge and decreased in length as angle of attack increased. Figure 8 plots the separation, transition, reattachment, and turbulent separation point histories with respect to angle of attack on the upper surface of the airfoil for $R_c = 200{,}000$, as determined from the pressure measurements and flow visualization data.

At the zero-lift condition $\alpha = -7$, laminar separation was found to occur at $x/c = 70\%$, with reattachment at 95%. As shown in Fig. 8 by 0-deg angle of attack, the separation point had moved forward to $x/c = 57\%$, with reattachment at $x/c = 83\%$. Between 0- and 8-deg angle of attack, the bubble moved upstream at a relatively constant rate, with very little change in bubble length. Between 8 and 12 deg, the laminar separation point moved upstream very rapidly, with bubble length remaining approximately constant (25% of x/c). As the angle of attack was further increased past 12 deg, upstream movement of the separation point slowed,

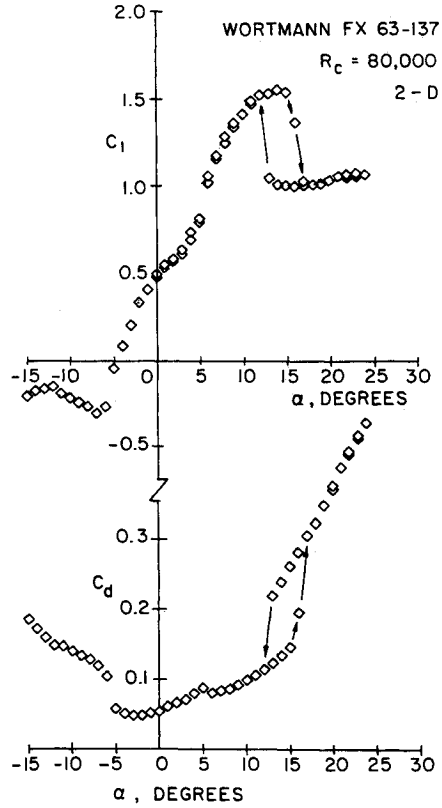

Fig. 3 Two-dimensional lift and drag coefficients vs angle of attack, $R_c = 80{,}000$.

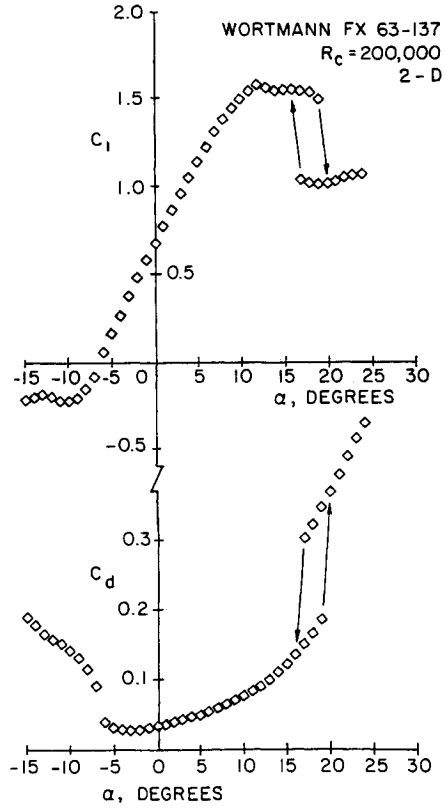

Fig. 4 Two-dimensional lift and drag coefficients vs angle of attack, $R_c = 200{,}000$.

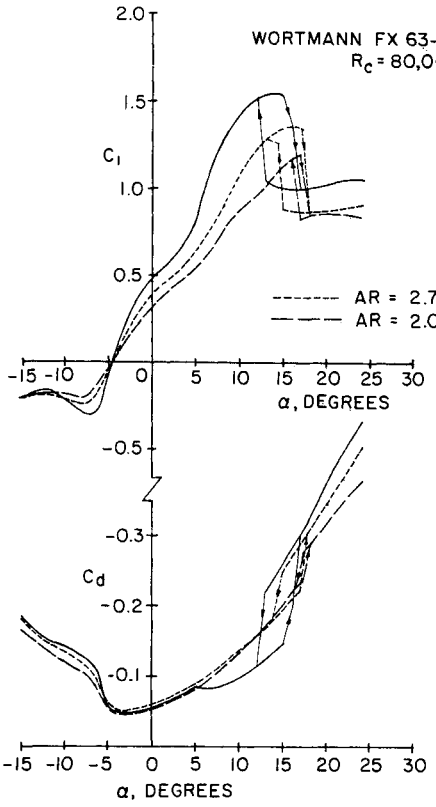

Fig. 5 Effect of aspect ratio on lift and drag coefficients at $R_c = 80{,}000$.

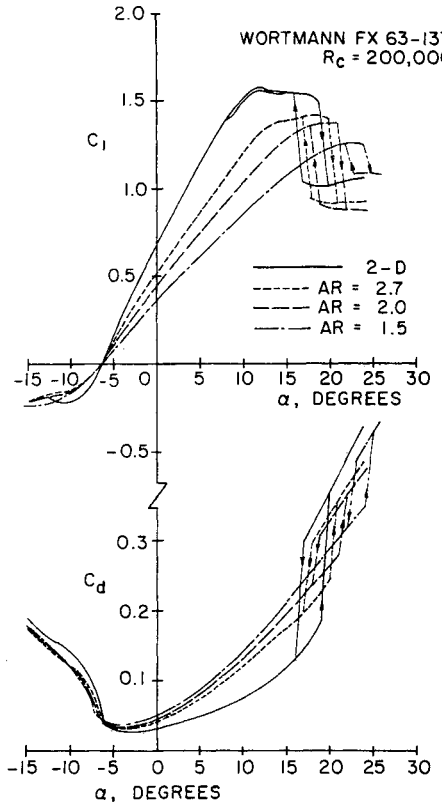

Fig. 6 Effect of aspect ratio on lift and drag coefficients at $R_c = 200{,}000$.

with the bubble length decreasing rapidly in this region. In general, as the angle of attack was increased, the separation, transition, and reattachment points moved upstream, with the bubble residing near the leading edge and becoming very short in length at high angles of attack. As the angle of attack was increased past 19 deg, the bubble burst, causing a dramatic decrease in lift, an increase in drag, and a clockwise hysteresis loop, as shown in Fig. 4.

An interesting phenomenon was noted in the pressure data for angles of attack greater than 11 deg. A pressure plateau, normally characteristic of the laminar separation bubble was not evident in some of the data. However, surface oil and smoke visualization indicated very clearly that separation bubbles existed on the upper surface for these angles of attack. It was soon recognized that the pressure taps were tripping the boundary layer. Figure 9 shows a comparison of in-line pressure taps to a staggered configuration. The tripping effect of the taps has two distinct consequences: the separation bubble effect is "washed out," and the suction peak is reduced in magnitude. Note that the two flows do converge to the same pattern after both flows have reached the reattached, fully turbulent state. This made the chordwise static-pressure distributions difficult to interpret for both the two-dimensional case and the spanwise distributions. This forced a heavier reliance on flow visualization data. All pressure data presented in this paper were obtained using the in-line tap configuration to obtain sectional characteristics along the span.

Spanwise Variation of the Laminar Separation on the $\mathcal{R} = 2.0$ Wing

Several cases will be presented to help describe the effect of the tip vortex on the laminar separation bubble on the upper surface. Every case shows that the tip vortex altered the upper surface flowfield by inducing an effective change in angle of attack along the span. Inboard (far from the vortex), the induced flow component in the spanwise direction was small; therefore, the airflow and boundary layers

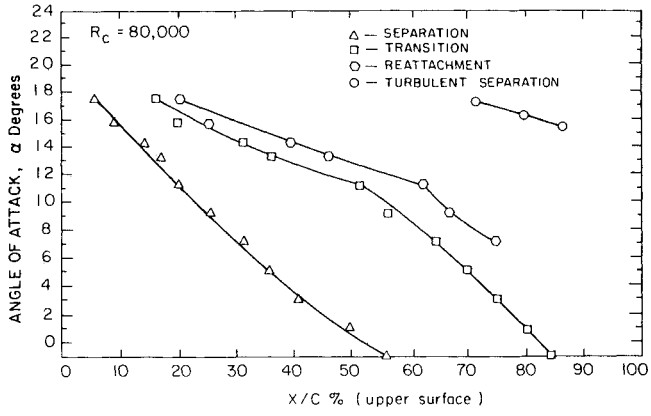

Fig. 7 Summary of laminar separation, transition, reattachment, and turbulent separation points, $R_c = 80{,}000$ (two-dimensional).

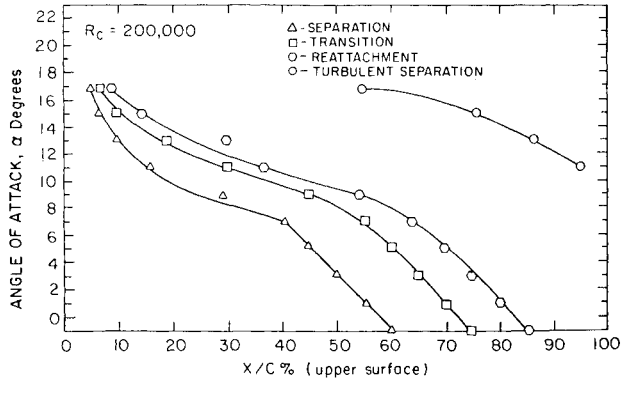

Fig. 8 Summary of laminar separation, transition, reattachment, and turbulent separation, $R_c = 200{,}000$ (two-dimensional).

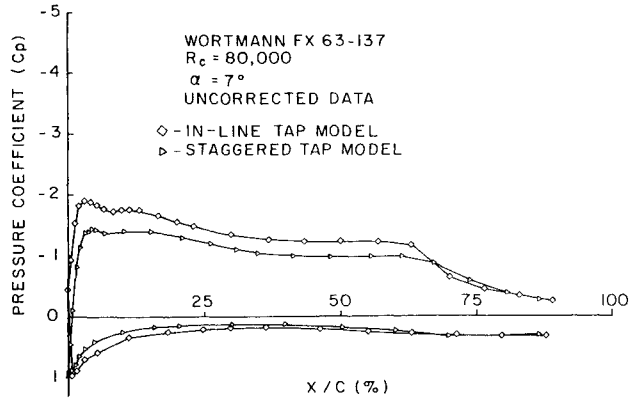

Fig. 9 Comparison of pressure distributions for the in-line and staggered-tap configurations, $R_c = 80{,}000$ and $\alpha = 7$ deg.

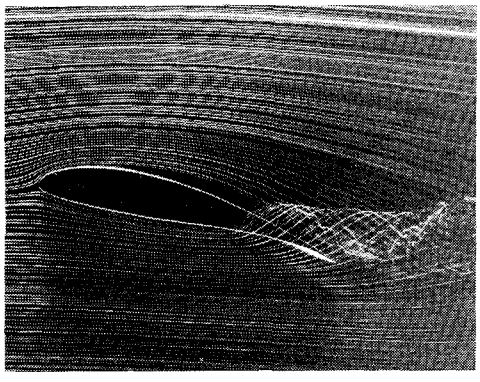

Fig. 10 Smoke-wire photograph of finite wing $\mathcal{R} = 2.0$ and $R_c = 80{,}000$, $\alpha = 14$ deg with the smoke introduced at the $y/b = 87\%$ position.

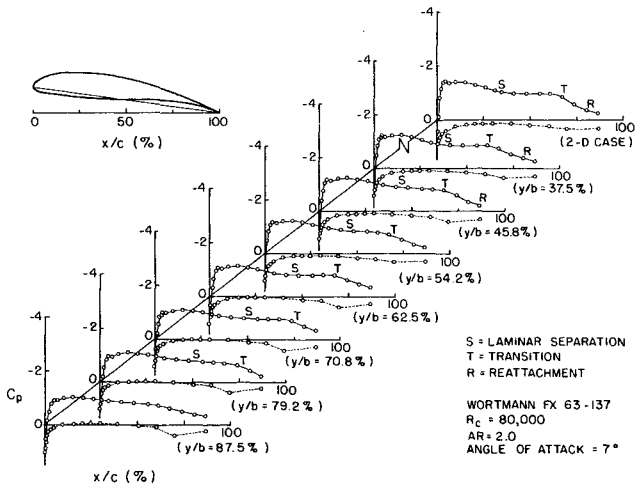

Fig. 11 Pressure distributions along the span, $R_c = 80{,}000$, $\alpha = 7$ deg, and $\mathcal{R} = 2.0$.

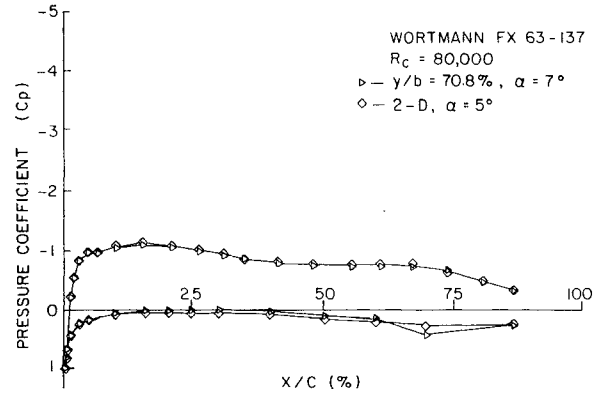

Fig. 12 Comparison of pressure distributions for $y/b = 70.8\%$ at $\alpha = 7$ deg and two-dimensional at $\alpha = 5$ deg, $R_c = 80{,}000$.

were primarily two-dimensional and could be approximated by airfoil data at the angle of attack equal to the effective angle of attack at that span station. Closer to the tip, a large spanwise flow component was induced by the vortex, modifying the chordwise pressure distributions greatly from the two-dimensional. Figure 10, a photograph from preliminary smoke-wire visualization, shows the tip vortex quite clearly. In this case, the smoke filaments were introduced at the $y/b = 87\%$ position (root to tip) on the $\mathcal{R} = 2.0$ wing at $R_c = 80{,}000$ and an angle of attack of 15 deg. The influence of the vortex was quite large, and the region of three-dimensional flow covered at least the outboard 20% of the wing.

Using the specially designed semispan pressure-tap model, it was possible to measure chordwise pressure distributions at seven stations along the span and also obtain two-dimensional airfoil data. These data, compared with the qualitative data obtained with a surface oil visualization technique, provided good descriptions of the upper surface flowfields on the $\mathcal{R} = 2.0$ wing.

The first case studied was the zero-lift condition at $R_c = 80{,}000$ (-5 deg). As expected, very little spanwise variation in the flowfield was observed on the upper or lower surface. Flow visualization showed that a tip vortex did not form, although there was some entrainment of both the upper and lower surface flows over the tip, due to the presence of the freestream. This effect proved to be beneficial, slightly increasing the sectional lift coefficients (determined by integrating chordwise pressure distributions obtained at each span station) near the tip.

A much more interesting case was an angle of attack of 7 deg, $R_c = 80{,}000$ (see Fig. 11). The wing lift coefficient was measured to be 0.65; thus it was expected that the influence of the tip vortex would be large. Indeed, inspection of the pressure distribution obtained on the wing verified this. Figure 11 plots the seven pressure distributions for the wing and the two-dimensional distribution for this case. The four inboard stations on the wing indicated turbulent reattachment points, and this was verified with flow visualization. Figure 12 is a comparison of the $y/b = 71\%$ pressure distribution with the two-dimensional distribution at 5-deg angle of attack. These show excellent agreement. Also, the airfoil data showed that between 5 and 7 deg, the long bubble collapsed to a short bubble, increasing airfoil performance.

A third case presented at this Reynolds number is an angle of attack of 17 deg shown in Fig. 13. Force balance data show that the two-dimensional case had just "stalled" while the wing lift coefficient was still increasing at an angle of attack of 17 deg. The measured wing lift coefficient for this case was 1.27. There was a large discrepancy in the pressure distributions between the two-dimensional case and the most inboard station on the wing, (i.e., $y/b = 38\%$), with a reduction in the suction peak and the integrated lift coefficient. Comparison with two-dimensional data showed that the three outboard stations had significant spanwise flow components, while the four inboard stations could be represented by two-dimensional pressure distributions at angles of attack less than 17 deg. Figure 14 is a sketch of the upper-surface flowfield based on pressure and surface oil visualization data. The similarity of this sketch to the flowfield proposed by Winklemann and Barlow[9] and Winklemann[10,11] in Fig. 15 allowed a reasonable level of confidence in these data.

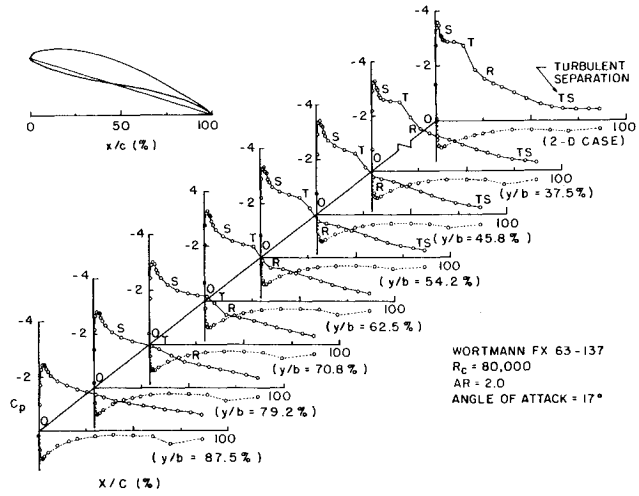

Fig. 13 Pressure distributions along the span, $R_c = 80{,}000$, $\alpha = 17$ deg, and $\mathcal{R} = 2.0$.

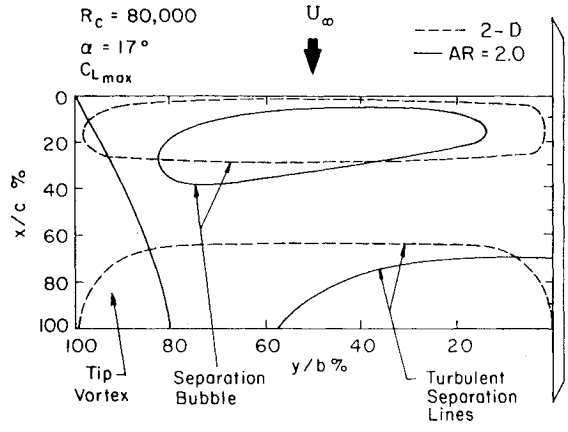

Fig. 14 Sketch of the upper-surface flowfield, $R_c = 80{,}000$, $\alpha = 15$ deg, and $\mathcal{R} = 2.0$.

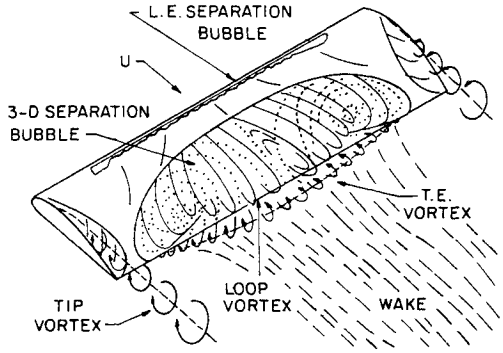

Fig. 15 Proposed flowfield for a rectangular planform wing at low Reynolds numbers, from Ref. 9.

Although the data obtained at $R_c = 200{,}000$ were of more interest because very few flight vehicles operate at Reynolds numbers as low as 80,000, the data were much more difficult to interpret, owing to the problems discussed earlier in this section. As was found at the lower Reynolds number, the zero-lift condition (-7 deg) showed very little variation in the chordwise pressure distributions along the span. There was, however, a slight improvement in performance near the tip, due to the entrainment of flow over the tip by the freestream.

Figure 16 is a plot of the lift coefficients obtained by integrating the pressure distributions along the span; thus, a

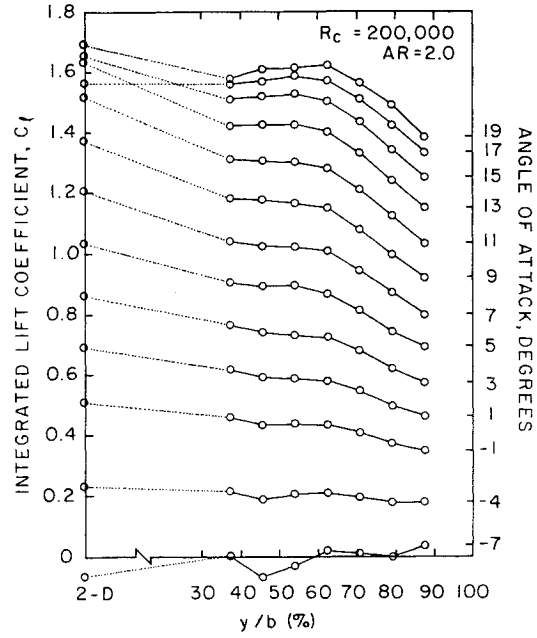

Fig. 16 Spanwise load distribution from integrating sectional pressure distributions, $R_c = 200{,}000$ and $\mathcal{R} = 2.0$.

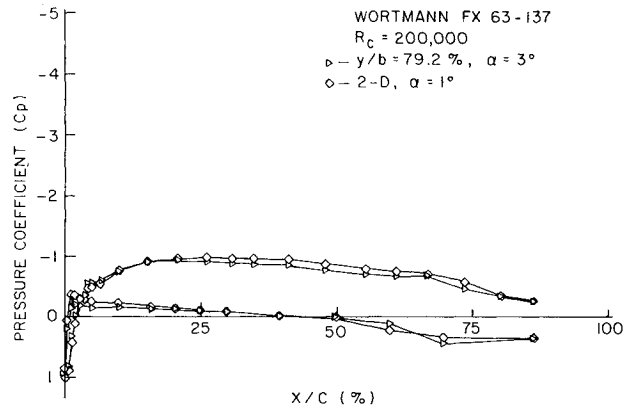

Fig. 17 Comparison of pressure distributions for $y/b = 79.2\%$ at $\alpha = 3$ deg and two-dimensional at $\alpha = 1$ deg.

spanwise load distribution for the $\mathcal{R} = 2.0$ wing at many angles of attack was generated. This plot shows very clearly the effect of the tip vortex and its increasing influence as angle of attack was increased. The figure indicates that the four inboard stations yielded nearly constant lift coefficients, while the three outboard stations yielded steadily decreasing lift coefficients. One should not infer from this that the flowfields were identical at the four inboard stations, but the integrated property was the same. Another interesting point to note is that although the four inboard stations produced nearly constant sectional lift coefficients, this value was substantially less than the two-dimensional value for angles of attack greater than 0 deg. This effect was also noticed at the lower Reynolds number.

By an angle of attack of 3 deg, a significant variation in the laminar separation point was noticed. Figure 17 is a comparison of the $y/b = 80\%$ span station with the two-dimensional distribution at 1-deg angle of attack. At $y/b = 38\%$, laminar separation occurred at $x/c = 40\%$ and was delayed to approximately $x/c = 60\%$ at $y/b = 80\%$.

As the angle of attack was further increased to 7 deg, the wing lift coefficient had increased to 0.9, and the influence of the tip vortex was much greater. Although Fig. 16 shows that the integrated lift coefficient was approximately con-

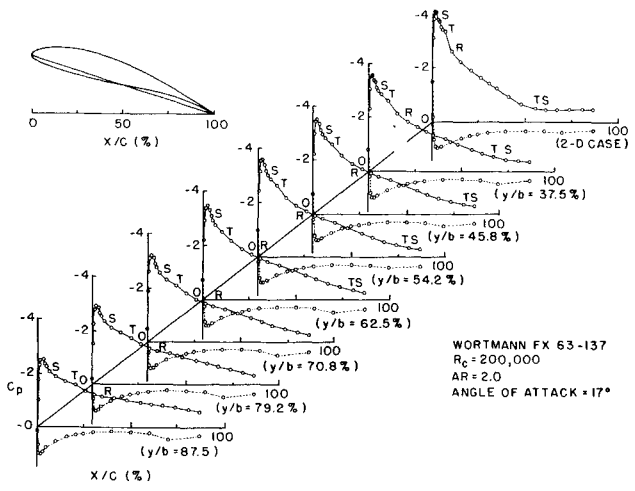

Fig. 18 Pressure distributions along the span, $R_c = 200{,}000$, $\alpha = 17$ deg, and $\mathcal{R} = 2.0$.

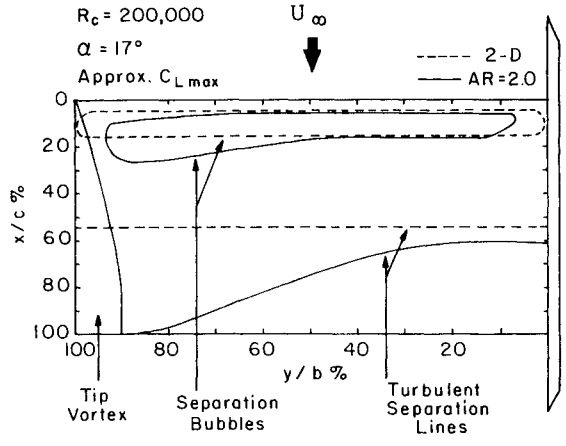

Fig. 19 Sketch of the upper-surface flowfield, $R_c = 200{,}000$, $\alpha = 17$ deg, and $\mathcal{R} = 2.0$.

stant from $y/b = 38$–62%, the pressure distributions show that the upper-surface flowfields were adversely affected by the tip vortex as early as $y/b = 45\%$. As occurred in all the previous cases, the reduction in the effective angle of attack resulted in a delay in laminar separation, coupled with an increase in separation bubble length. The shortening of the bubble near the tip (the last two stations in particular) was due to the increasingly three-dimensional flow in that region.

The last case presented is an angle of attack of 17 deg, $R_c = 200{,}000$. The pressure distributions along the span were difficult to interpret (Fig. 18), but careful comparison of this with flow visualization data allowed the upper-surface flowfield to be sketched (Fig. 19). As in the case near maximum lift at the lower Reynolds number, this flowfield was similar to that of Winklemann, with a single, large, separated "cell" forming after turbulent separation.

Concluding Remarks

A study of the two-dimensional airfoil characteristics was performed to generate a data base for comparison to the data obtained for the finite wing. It was found that in the Reynolds number range studied, performance could be divided into two categories. The first case, Reynolds numbers less than 150,000, was characterized by the highly nonlinear lift curves. In the second range, Reynolds numbers greater than 150,000, the slopes of the lift curves became more linear and began to converge to one shape. This shape was similar to that published in Ref. 12 for a chord Reynolds number of 500,000. Comparison of these two-dimensional data to those of Althaus showed a good correlation for the lift coefficient. There were large discrepancies between drag coefficients measured. The possible reasons for the discrepancies are the different testing methods and testing environment.

At the lower Reynolds number, $R_c = 80{,}000$, the rapid formation of a separation bubble on the upper surface near $\alpha = 7$ deg caused a large jump in lift coefficient and a decrease in drag coefficient. The condition of laminar separation without turbulent reattachment existed at angles of attack less than 7 deg. In these cases, the laminar flow separated from the upper surface since it could not negotiate the adverse pressure gradient. The free laminar shear layer traveled downstream approximately parallel to the freestream, and transition occurred, yielding a highly circulatory turbulent flow. This flowfield closely resembled leading-edge separation, except that the separation occurred at chord positions ranging from 70% x/c at $\alpha = -5$ deg to 35% x/c at $\alpha = 5$ deg, not at the leading edge.

When the separation bubble formed, the flowfield underwent a drastic change. A suction peak began to form in the pressure distributions, with the bubble moving upstream and decreasing in length as incidence was increased. At approximately $\alpha = 13$ deg, the separation bubble resided near the leading edge and behaved as a traditional short separation bubble would.

At the higher Reynolds number, the change in the separation bubble on the upper surface with angle of attack was not as drastic; thus, the lift curve became more linear. The upper surface bubble formed initially at $\alpha = -7$ deg near the angle of zero lift. It covered 30% of the upper surface when it formed, and it became shorter with increasing incidence. Between angles of attack of 7-11 deg, the separation point moved forward rapidly, and flow visualization showed the bubble to be very "thin." In this range, it was very difficult to identify separation bubble location from pressure distributions, although identification was clear with laser light and smoke visualization. As occurred with the lower Reynolds number, the separation bubble moved upstream near the leading edge at angles of attack greater than 13 deg and became shorter with increasing incidence. At this point, the separation bubble acted primarily as a boundary-layer trip, modifying the surface geometry very little but causing a thick, attached, turbulent boundary layer to form. As angle of attack was increased past the maximum lift coefficient, lift production remained constant.

The performance of the three rectangular wings was determined as a function of chord Reynolds number *and* wing aspect ratio. These data were then compared to the two-dimensional data. The formation and movement of the separation bubble were studied on one wing ($\mathcal{R} = 2.0$) at two chord Reynolds numbers: 80,000 and 200,000. These studies were similar to those performed in the two-dimensional cases, but spanwise variation in effective angle of attack was introduced as an additional parameter.

It was found that increasing chord Reynolds number had the same effects on the wings that it did on the airfoil section. The maximum values of lift coefficient and performance ratios increased as Reynolds number increased, while the minimum drag coefficient decreased. Again, the Reynolds number range could be divided into a rapidly changing region ($R_c < 150{,}000$) and a relatively constant region ($R_c > 150{,}000$). The changes in the performance parameters with respect to Reynolds number were smaller as aspect ratio was decreased. Increasing the aspect ratio of a wing increased the lift curve slope.

At both Reynolds numbers, it was determined that separation bubble formation and motion on the wing was analogous to bubble formation in two dimensions. The only difference was that as the effective angle of attack was reduced along the span, the bubble behaved locally according to the effective angle of attack. Thus, separation bubbles

on the finite wing had curved lines of separation as spanwise stations near the tip saw an effectively reduced angle of attack. This was verified by comparing two-dimensional pressure distributions with those at wingspan stations.

The data presented were the result of an investigation into the performance of wings at low Reynolds numbers and the effect of the tip vortex on the separation bubbles on the upper surface. The data collected showed promise that low Reynolds number wing performance and the spanwise flowfield variation can be collected and possibly predicted by analytic methods.

Acknowledgments

This research was supported by the Office of Naval Research under Contract N00014-83-K-0239 and the Department of Aerospace and Mechanical Engineering, University of Notre Dame.

References

[1]Arena, A.V. and Mueller, T.J., "On the Laminar Separation, Transition, and Turbulent Reattachment of Low Reynolds Number Flows Near the Leading Edge of Airfoils," AIAA Paper 79-0004, 1979.

[2]Mueller, T.J. and Batill, S.M., "Experimental Studies of the Laminar Separation Bubble on a Two-Dimensional Airfoil at Low Reynolds Numbers," AIAA Paper 80-1440, 1980.

[3]Jansen, B.J., "Experimental Studies of the Effect of the Laminar Separation Bubble on the Performance of a NACA 663-018 Airfoil at Low Reynolds Numbers," M.S. Thesis, University of Notre Dame, Notre Dame, IN, 1982.

[4]Pohlen, L.J., "Experimental Studies of the Effect of Boundary Layer Transition on the Performance of the Miley (MO6-13-128) Airfoil at Low Reynolds Numbers," M.S. Thesis, University of Notre Dame, Notre Dame, IN, 1983.

[5]O'Meara, M.M., "An Experimental Investigation of the Separation Bubble Flow Field Over an Airfoil at Low Reynolds Numbers," M.S. Thesis, University of Notre Dame, Notre Dame, IN, 1985.

[6]Bastedo, W.G. Jr., "Performance of an Airfoil and Three Rectangular Planform Wings at Low Reynolds Numbers," M.S. Thesis, University of Notre Dame, Notre Dame, IN, 1985.

[7]Tani, I., "Low Speed Flows Involving Bubble Separations," *Progress in Aeronautical Sciences,* Vol. 5, Macmillan, New York, 1984, Chap. 2.

[8]Mueller, T.J., "The Influence of Laminar Separation and Transition on Low Reynolds Number Airfoil Hysteresis," AIAA Paper 84-1617, June 1984.

[9]Winklemann, A.E. and Barlow, J.B., "A Flowfield Model for a Rectangular Planform Wing," *AIAA Journal,* Vol. 18, Aug. 1980, pp. 1006-1008.

[10]Winklemann, A.E., "An Experimental Study of Mushroom-Shaped Stall Cells," AIAA Paper 82-0942, June 1982.

[11]Winklemann, A.E., "An Experimental Study of Separated Flow on a Finite Wing," AIAA Paper 81-1882, Aug. 1981.

[12]Althaus, D., *Profilpolaren für den Modellflug*, Neckar-Verlag, Berlin, 1982.